COBEM 2023 27TH INTERNATIONAL CONGRESS OF MECHANICAL ENGENEERING

ABCM Brazilian Society of Mechanical Sciences and Engineering
27th ABCM International Congress of Mechanical Engineering
December 04-08, 2023, Florianópolis-SC, Brazil

COB-2023-0617
COMPUTER VISION AND THREE DIMENSIONAL PROFILOMETRY APPLIED TO CORROSION DETECTION IN DEEP ROLLED AISI 1045 STEEL

Gabriel Ferraz Vieira
Mechanical Engineering Undergraduate Program, Universidade Federal de Minas Gerais, Avenida Antônio Carlos 6627, Belo Horizonte, MG 31270-901, Brazil
e-mail: gabrielferraz163@gmail.com

Vinícius Melo Cangussu
Alexandre Mendes Abrão
Graduate Program in Mechanical Engineering, Universidade Federal de Minas Gerais, Avenida Antônio Carlos 6627, Belo Horizonte, MG 31270-901, Brazil
e-mails: viniciusmelocangussu@gmail.com, abrao@ufmg.br

Abstract. *Metallic components are designed to operate under distinct environments, which may expose the materials to all sort of adversities. Among these adversities is corrosion, an ordinary process that can decrease the lifespan and impair the performance of components. The main goal of this research is to investigate the influence of deep rolling feed on the corrosion resistance of forged AISI 1045 steel (average hardness of 212 HV) and to propose alternative approaches to identify corrosion on the surface of materials. After deep rolling with distinct feed values, the specimens were subjected to corrosion tests in a 3.5% NaCl aqueous solution for 72 hours. A computer vision algorithm, based on the Python programming language, and three-dimensional profilometry were employed to identify and evaluate the surface of the deep rolled samples. The results indicate that deep rolling was able to modify the corrosion behavior, i.e., as the deep rolling feed rate decreases, the density and depth of pits decrease. Furthermore, the developed algorithm is capable of identifying and counting the contours of points and small areas formed by localized corrosion using optical microscopy images.*

Keywords: *Deep rolling, Python language, corrosion analysis, AISI 1045 forged steel.*

1. INTRODUCTION

The corrosive process, in general, is spontaneous and represents undesirable changes in materials, such as wear, chemical variations, or structural modifications. As a typically spontaneous process, corrosion holds significant importance to modern life, deteriorating metallic structures such as water and gas pipelines, slurry pipelines, airplanes, automobiles, heat exchangers, among others (Gentil, 2011). The mechanisms governing corrosion adhere to well-established principles, and in the case of metals, it occurs through oxidation-reduction reactions, wherein electrochemical reactions between the metal and the environment take place in the form of electron transfer. In this case, it is said that the metal oxidizes by releasing electrons to an oxidizing agent (the corrosive substance). As corrosion is generally a surface reaction, considering surface alterations is relevant when investigating the corrosive process. Another aspect to consider is that the metallic compound formed by corrosion can act as a barrier between the corrosive environment and the metal, thereby reducing the corrosion rate.

Among the different forms of corrosion, pitting corrosion is of great importance when assessing the performance and service life of metals. According to Sheir (1994), pitting corrosion is the most common form of corrosion and often leads to perforation and corrosion failure. Pitting corrosion is an extremely localized form of corrosion that typically occurs randomly, isolated or grouped, resembling generalized corrosion. Due to its localized nature, evaluating pitting corrosion is challenging due to either the oxide layer that may conceal it or the variable size and depth of the pits. According to Sheir (1994), the surface conditions of the metal are an important factor in assessing localized corrosion, since crystal defects and structural characteristics can affect the thickness, adhesion, porosity, composition, and solubility of the surface films formed during corrosion.

There are several techniques used to protect metals from corrosion. One of the main techniques is the application of protective coatings, such as paints and enamels, which form a physical barrier between the metal and the corrosive environment. Another common technique is galvanization, which involves coating the metal with a layer of zinc, providing sacrificial protection. In addition to coating, there are also ways to protect the material by modifying the oxidation-reduction process, such as cathodic protection. However, surface treatment of the metal remains fundamental in corrosion protection.

Deep rolling is a mechanical surface treatment capable of improving surface finish (reducing roughness), generating compressive residual stresses, improving fatigue strength, and achieving precise dimensions in the workpiece (Schulze, 2006). In deep rolling, a rolling element is pressed against the workpiece with a defined pressure. The applied force causes plastic deformation near the material's surface. This process is employed in the automotive industry, general mechanics, and extensively in aircraft construction (Schulze, 2006).

During deep rolling, the rolling element deforms the surface roughness peaks and displaces the material into the valleys (Chomienne et al., 2016). According to Abrão et al. (2014), the rolling element can be pressed against the workpiece using springs or other mechanical elements, but the use of hydrostatic pressure is the principal method due to the fact that elastic deformation is avoided. The parameters that can be controlled in deep rolling are force or pressure, speed, feed, number of passes, and rolling element material and diameter (Delgado et al., 2015).

Saldaña-Robles et al. (2018) demonstrated that deep rolling was able to increase the corrosion resistance of AISI 1045 steel. Through electrochemical impedance testing (EIS), they concluded that the turned samples exhibited 12 times higher charge-transfer resistance compared to deep rolled samples. Gharbi et al. (2021) also reported that deep rolling increased the corrosion resistance of AISI 304 stainless steel, primarily due to a combination of factors inherent to the process, such as surface hardness, microhardness, grain recrystallization, and induction of residual stresses. Similarly, Al-Qaeabeha et al. (2009) reported that deep rolling can significantly increase the corrosion resistance by producing a fine-grained structure on the surface of A53 steel. According to Pu et al. (2011), the grain refinement mechanism occurs due to dynamic recrystallization. Although the corrosion mechanism differs in stainless steels compared to carbon steels, corrosion in carbon steel occurs in a similar way. While both materials can corrode, stainless steels are more corrosion-resistant than carbon steel due to the presence of a passive layer of chromium oxide. This protective layer allows stainless steels to better withstand corrosive environments, such as exposure to saltwater or corrosive chemicals.

The effect of deep rolling process on corrosion resistance can be evaluated using many techniques, such as electrochemical impedance spectroscopy (EIS), electron work function (EWF), electron backscattered diffraction (EBSD) potentiodynamic polarization (Tafel), galvanostatic techniques, potentiostatic polarization or Mott-Schottky plots (Jinlong et al., 2013, 2016). However, the evaluation of corrosion resistance using image processing techniques, computer vision and three-dimension profilometry has not been reported in the literature to date.

Image processing encompasses a wide range of techniques, from basic preprocessing operations, such as filtering and histogram equalization, to more advanced algorithms, such as edge detection, geometric transformations, segmentation, and pattern recognition. These techniques allow extracting relevant information from images, making them more understandable and useful for analysis. Likewise, computer vision incorporates and applies image processing techniques to enable automated evaluation of visual content in images. This allows computers to interpret and understand the visual world similarly to humans but with the ability to handle large volumes of data quickly and efficiently, thereby identifying information that might go unnoticed in human analysis.

In this study, image processing techniques, computer vision, and contact profilometry were employed to qualitatively evaluate pitting corrosion on the surface of forged AISI 1045 steel after undergoing deep rolling and being subjected to a corrosion test in a saline solution.

2. METHODOLOGY

In this section, the materials, equipment, and methodology used to conduct this research will be presented. The steps corresponding to the methodology are outlined in the flowchart shown in Figure 1 and described below.

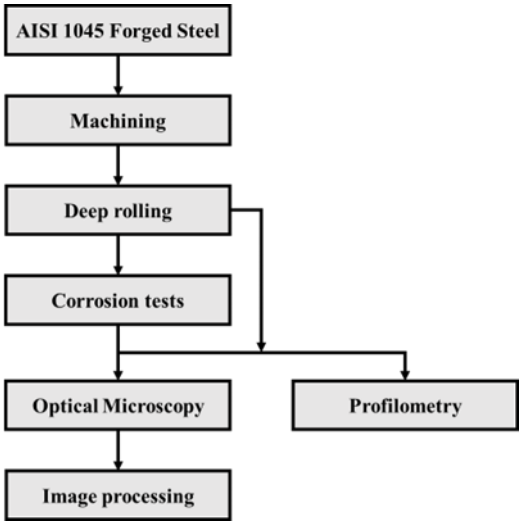

Figure 1. Methodology.

2.1 Material and methods

Cylindrical bars of forged AISI 1045 steel (average hardness of 212 HV) with a diameter ranging from 17 to 20 mm and length of 700 mm were used as work material. The chemical composition was obtained through optical emission spectrometry (iron-based), see Table 1.

Table 1. Chemical composition (% weight) of AISI 1045 steel.

Elements	Concentration
Carbon (C)	0.4866
Silicon (Si)	0.1839
Manganese (Mn)	0.7529
Phosphorus (P)	0.0228
Sulfur (S)	0.0111
Chromium (Cr)	0.0270
Molybdenum (Mo)	0.0110
Copper (Cu)	0.0107
Iron (Fe)	98.3808
Others	0.1132

Dry machining of the specimens was conducted on a CNC lathe (power of 5.5 kW and maximum rotational speed of 3,500 rpm) using Mitsubishi VCMT 160408 UE6110 inserts with a TiCN-Al_2O_3-TiN multilayer coating, mounted on a SVVCN 2020-K16N tool holder. Rough turning was performed at a constant cutting speed of 45 m/min, a feed rate of 0.20 mm/rev, and depth of cut of 1.0 mm. Subsequently, finish turning was carried out at a cutting speed of 40 m/min, a feed rate of 0.10 mm/rev, and maximum depth of cut of 0.25 mm. After turning, specimes with a diameter of 10 mm and 230 mm long were obtained.

After machining, the samples were subjected to deep rolling on the same lathe previously described, using an Ecoroll HG6-20 hydrostatic deep rolling tool with three 6 mm diameter balls spaced 120° apart. Petronas Mecafluid S3000 synthetic fluid was used at a concentration of 10% in water. The selected deep rolling parameters were as follows: speed of m/min, pressure of 90 bar, and feed rates of 0.04, 0.08, and 0.12 mm/rev. Four replicates were performed for each condition. The pressure of 90 bar was chosen based on the steel hardness (Ecoroll, 2016).

After deep rolling, the samples were soaked in a 3.5% NaCl solution for 72 hours. A rotating device was responsible for keeping the samples in constant motion within a homogeneous solution. Sodium chloride was selected due to its strong electrolyte nature, leading to an increase in conductivity, which is essential for the electrochemical corrosion mechanism. In the case of iron corrosion in air-saturated water at room temperature, it is observed that the corrosion rate initially increases with the concentration of sodium chloride and then decreases, with the maximum rate occurring at 3.5% NaCl (Gentil, 2011). This concentration is near the concentration of seawater and was chosen for its effectiveness in the corrosive process.

After corrosion, an Olympus CX31 optical microscope was used to capture the images of the deep rolled surfaces with and without corrosion. Each image corresponds to an area of 650.4 by 486.6 µm. Finally, a Hommelwerke Hommel Etamic T8000 profilometer was used to generate three-dimension topographic images of the samples surface. By using contact profilometry, detailed information related to the surface of a material, including its roughness, irregularities, and other relevant parameters can be obtained. Profilometry was conducted using a probing length of 10 mm, width of 3 mm and a step of 10 µm.

2.2 Image processing and profilometry

An image can be described as a two-dimensional function $f(x, y)$, where x and y are spatial coordinates, and the amplitude of f at any pair of coordinates (x, y) is the intensity or grayscale level of the image at that point. When x, y, and intensity values are finite and discrete, one has a digital image (Gonzalez et al., 2010). Image processing focuses on performing operations on digital images to accomplish tasks such as color correction, noise removal, edge detection, object segmentation, pattern recognition, among others.

The techniques used in image processing can range from basic operations such as filtering and histogram equalization to more complex algorithms involving machine learning and statistical processing. In this work, all applied algorithms are based on the Python programming language in conjunction with the Open Source Computer Vision library (OpenCV, 2023). Python is a programming language that provides an efficient data structure and a simple yet effective approach to object-oriented programming. Python is considered a language that combines capabilities and functionalities with a very clear code syntax, and it is equipped with a comprehensive and extensive standard library (Summerfield, 2010).

The OpenCV library has a primary focus on image manipulation and processing, providing a wide range of algorithms and tools for visual data analysis and interpretation. Its flexible and modular architecture allows rapid and efficient

development of computer vision applications, with support for multiple programming languages. OpenCV is widely used in various fields such as robotics, industrial automation, security, augmented reality, and facial recognition, offering advanced features for real-time object detection, tracking, segmentation, and recognition (OpenCV, 2023).

One of the main difficulties related to image processing of metallic surfaces is concerned with the treatment and filtering of images, since the corroded metal presents an oxide layer resulting from corrosion, which complicates and introduces noise to the image. However, all the challenges faced in processing microscopy images represent one of the main contributions of this research, which is to develop versatile techniques using relatively simple equipment that can deliver satisfactory performance even with low-quality images.

Figure 2 presents the processing steps developed in this work. The first step in image processing, is to convert the color scale (Figure 2a) to grayscale (Figure 2b). This step simplifies the image, reducing both processing time and hardware requirements. This conversion step is also important because it allows the image to undergo thresholding processes and ensures color standardization even if the input is in color.

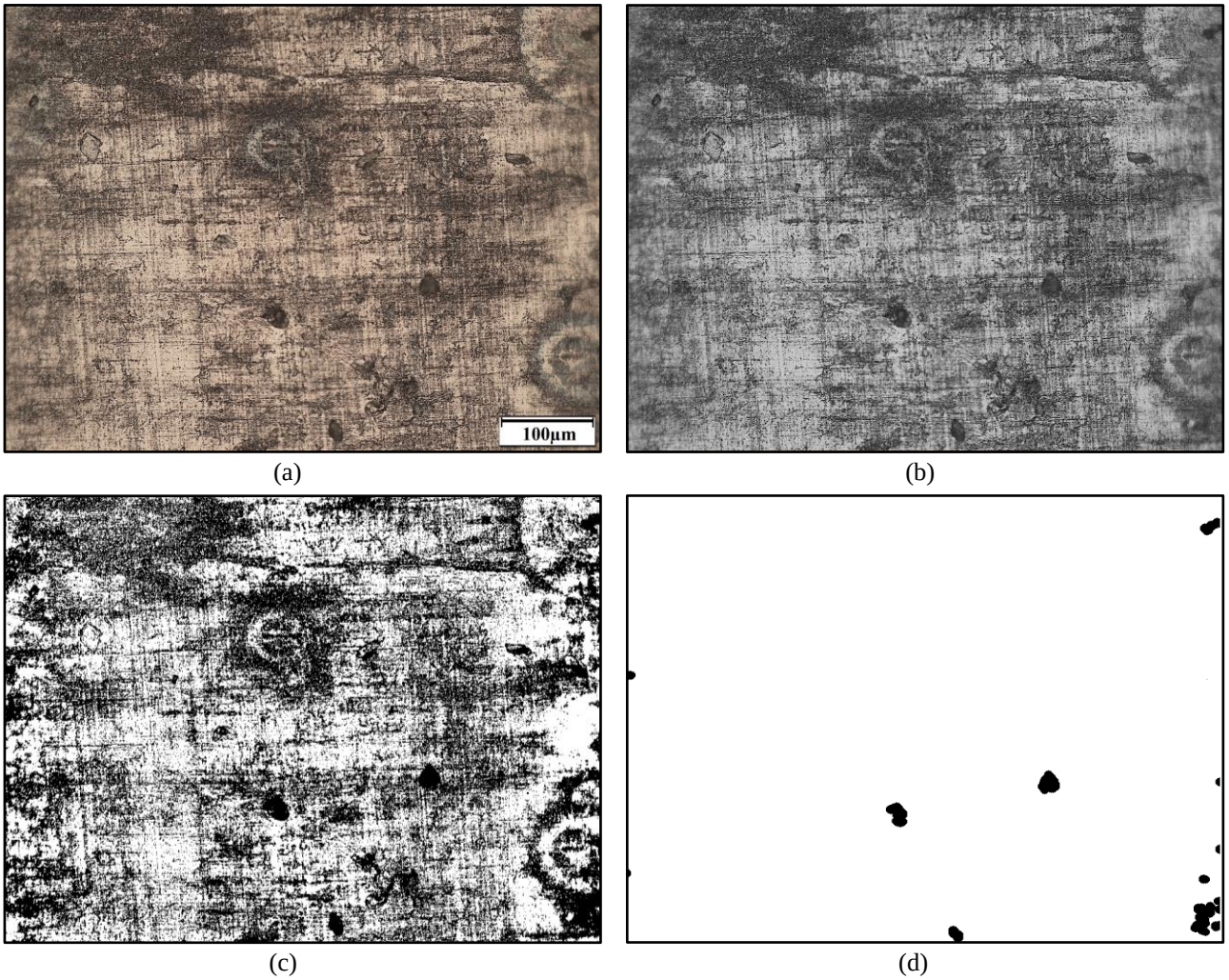

Figure 2. Image processing: (a) original image, (b) grayscale conversion, (c) adaptive thresholding, (d) morphological processing.

After converted to grayscale, the image is ready to undergo thresholding (Figure 2c). Thresholding consists of separating the regions of an image when it presents two classes: the background and the object. Since thresholding produces a binary image (only black and white pixels) as output, it is often referred to as binarization. The simplest form of thresholding involves partitioning the histogram by converting pixels with a grayscale value greater than or equal to a certain threshold value to white, and the remaining pixels to black. The histogram of an image is a set of numbers that indicates the percentage of pixels in the image with a specific grayscale level. By visualizing the histogram of an image, one can obtain an indicative of its quality in terms of contrast level and average brightness (whether the image is predominantly light or dark).

The OpenCV library provides a type of thresholding called adaptive thresholding. Unlike global thresholding, where a single threshold value is applied to the entire image, adaptive thresholding considers different thresholds for different

regions of the image, taking into account local variations in illumination, contrast, and noise. Adaptive thresholding involves subdividing the image into smaller regions (windows) and determining the optimal threshold value for each region based on a local threshold function. This local threshold function can be a weighted average of the pixel intensity levels in the region or a statistical analysis such as mean or median. After thresholding, the pit has more pronounced edges with a higher number of black pixels, see Figure 2c. However, the same occurs to others regions that are not of interest, where imperfections on the steel surface are also enhanced, although to a lesser extent.

Adaptive thresholding is particularly useful in cases where the image illumination is irregular or variable and when there are details of different sizes or contrasts in different regions of the image, such as corrosion pits. It allows for more precise segmentation, preserving low-contrast details and minimizing the influence of noise and global variations in the image. In the algorithm, there are two parameters that control adaptive thresholding: the block size and the subtraction constant (C). The block size determines the local area around each pixel used to calculate the adaptive threshold value. Larger block sizes take into account a larger region around each pixel, which can be useful in cases of images with smoother illumination variations or smoother gradients. On the other hand, smaller block sizes are more suitable for detecting fine details or abrupt illumination variations. The subtraction constant (C) is used to adjust the calculated adaptive threshold value. It is subtracted from the mean or weighted value of the pixel's neighborhood, depending on the chosen method. Positive values of C make the binarized image brighter, while negative values make it darker.

The chosen values for the block size and subtraction constant were based on experimental tests. Since the images presented specific noises and intensities, mainly due to the image acquisition method using an optical microscope, higher block sizes proved to be more effective as they consider a larger region around each pixel, smoothing out small details. In the case of the subtraction constant, small positive values better suited the images, effectively brightening the binarized image and reducing smaller noises.

Following with the treatment of the binarized image, a more complex step called kernel, also from the OpenCV library, is applied (Figure 2d). A kernel is a matrix or filter matrix that is applied to an image to perform convolution or filtering operations. The kernel defines how each pixel in the input image will be combined with its neighboring pixels to calculate the resulting value in the output image. The size and shape of the kernel determine the type of operation that will be applied to the image. For example, a smoothing kernel (also known as an average kernel) is a square matrix with equal values, which is used to perform the smoothing operation, where each resulting pixel is a weighted average of the values of neighboring pixels. Another example is the edge detection kernel, which is used to enhance edges or transitions in the image. These kernels are designed to identify abrupt differences in pixel intensity values in different regions of the image. There are various types of kernels available, including smoothing, edge detection, sharpening, blurring, among others. Each type of kernel is designed to perform a specific image processing task. Proper use of the kernel can help enhance desired features, remove noise, detect edges, and perform various other image processing operations.

The presence of noise from the thresholding step (Figure 2c) is evident. Therefore, the application of morphological processing through the kernel, see Figure 2d, proved to be suitable as it allowed for morphological transformation of closing, where the kernel was used to fill gaps and smooth the edges of the pit. Since the pits are relatively small points in the image, smaller values for the kernel proved to be more effective, as the edges were smoothed more intensely.

With the filtered images, the computer vision algorithm for edge detection and pit counting is applied. The algorithm used, present within the OpenCV library, was the SimpleBlobDetector. The SimpleBlobDetector algorithm is used to identify regions of interest in the image that have a distinct appearance, such as spots or objects with approximately circular shapes. Its operation is based on searching for regions that meet certain user-defined criteria, such as size, shape, color, and other attributes. These criteria are specified through adjustable parameters that can be configured according to the specific characteristics of the pits to be detected. Since the pits have well-defined contours, after the filtering step, the algorithm can be applied.

3. RESULTS

For each deep rolling condition, 15 images of the steel surface were captured by the optical microscope. In total, 90 images were subjected to the algorithm for corrosion evaluation. In Figure 3, it is possible to visualize the pits identified and highlighted in red by the algorithm.

Figure 3. Identification of pits by the algorithm.

As previously mentioned, the oxides formed during the corrosive process are one of the main challenges in pit identification, since they not only generate noise in the image, but can also conceal the corrosion pits. The results obtained for all conditions are presented in Figure 4.

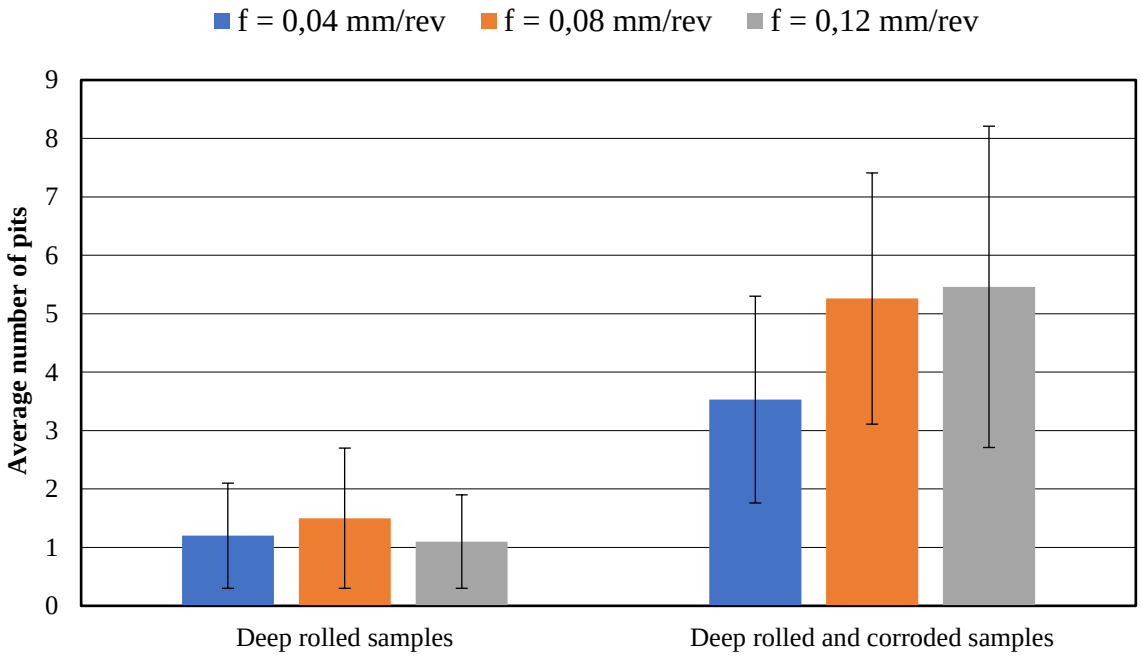

Figure 4. Algorithm results for pit count.

Not surprisingly, the number of pits increased substantially after the corrosion test. Moreover, the number of pits of the deep rolled and corroded samples increased with feed rate. However, some pits were not detected by the algorithm, mainly due to the image quality. Additionally, contour-like features (material defects) resembling pits were detected on the images of the deep rolled samples not subjected to corrosion, but in lesser quantity compared to the corroded samples.

In addition to the algorithm-based evaluation, the profilometry analysis showed differences in the corrosion behavior of the material. Figures 5a and 5b show, respectively, the topography of a sample deep rolled with a feed rate of 0.04 mm/rev before and after the corrosion test. In the former, no visible imperfections or defects are present on the metal. On the other hand, the latter clearly shows pits randomly dispersed. The maximum pit depth recorded in Figure 5b was 9.53 µm, which is deeper than the maximum depth measured in Figure 5a (1.99 µm). Similarly to the algorithm results, an increase in the number of pits on the metal surface is observed as the feed rate is further increased to 0.08 and 0.12 mm/rev. For a feed rate of 0.08 mm/rev, the feed marks are the only features observed before corrosion (Figure 5c). After the corrosion (Figure 5d), however, an increase in both the number of pits and in the maximum depth is observed, with

the latter reaching 14.1 µm. This result suggests that increasing feed rate leaves a larger portion of the material untreated by deep rolling, exposing a larger undeformed area to the corrosive environment.

After deep rolling with a feed rate of 0.12 mm/rev (Figure 5e), the feed rate marks become more evident, and yet the surface does not exhibit any visible defects. After the corrosion test (Figure 5f), an increase in the number of pits is observed, but the maximum depth found was slightly lower compared to a feed rate of 0.08 mm/rev. In this condition, the deepest pit detected by the profilometer was 9.57 µm deep.

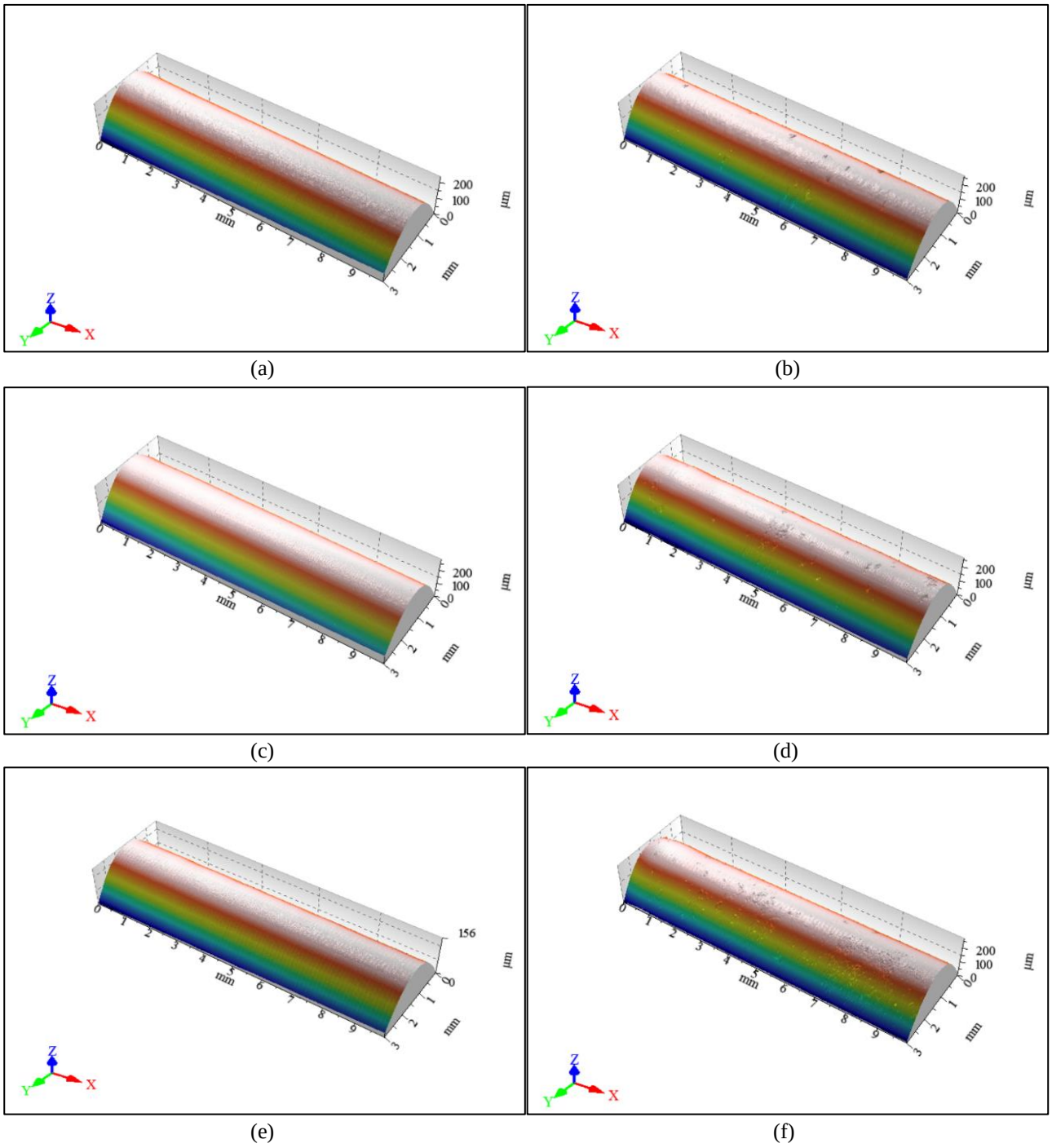

Figure 5. Profilometry images of deep rolled (DR) samples: (a) DR at 0.04 mm/rev before the corrosion test, (b) DR at 0.04 mm/rev after the corrosion test, (c) DR at 0.08 mm/rev before the corrosion test, (d) DR at 0.08 mm/rev after the corrosion test, (e) DR at 0.12 mm/rev before the corrosion test and (f) DR at 0.12 mm/rev after the corrosion.

4. CONCLUSION

Based on the presented findings, it can be concluded that the increase in deep rolling feed rate elevates the number of pits is forged AISI 1045 samples subjected to corrosion tests.

Moreover, the algorithm used for the detection of corrosion pits presented a satisfactory performance. Due to its operation based on criteria such as circularity, area, convexity, among others, the algorithm exhibits significant versatility in defining what should be identified in the image, making it possible to expand its application to the detection of other objects. Furthermore, all the discussed filtering steps can be extended to more complex algorithms, including machine learning, as the main challenge in applying computer vision for detection lies in the quality of the presented object of interest.

The presence of oxides posed the greatest challenge in image processing for pit detection, as it increased the amount of noise and concealed the pits.

The results from the contact profilometry measurements confirmed those from the developed algorithm, i.e., the lowest deep rolling feed rate (0.04 mm/rev) provided highest resistance to corrosion (least number of pits per image), due to the fact that the plastically deformed areas are overlapped as the tool travels.

5. REFERENCES

Abrão, A. M., Denkena, B., Breidenstein, B., Moerke, T., 2014, Surface and subsurface alterations induced by deep rolling of hardened AISI 1060 steel, Prod. Eng. Res. Devel. vol. 8. p. 551–558.

Al-Qawabeha, U., Al-Rawajfeh, A.E., Al-Shamaileh, E., 2009, Influence of roller burnishing on surface properties and corrosion resistance in steel, Anti-Corros. Methods Mater., Vol. 56, p. 261–265.

Chomienne, V., Valiorgue, F., Rech, J., Verdu, C., 2016, Influence of ball burnishing on residual stress profile of a 15-5PH stainless steel, CIRP Journal of Manufacturing Science and Technology, Vol.13, p. 90–96.

Delgado, P., Cuesta, I.I., Alegre, J.M., Díaz, A., 2015, State of the art of Deep Rolling. Precision Engineering, Vol. 46, p. 1–10.

Ecoroll, 2016, Tool Technology for Metal Surface Improvement: Solutions for a Demand oriented Surface Quality.

Gentil, V., 2011, Corrosion, LTC, 6th edition (In Portuguese).

Gharbi, K., Ben Moussa, N., Ben Rhouma, A. et al., 2021, Improvement of the corrosion behavior of AISI 304L stainless steel by deep rolling treatment under cryogenic cooling, Int. J. Adv. Manuf. Technol., Vol 117, p. 3841–3857.

Gonzalez, R. C., Woods, R. E., 2010, Digital Image Processing, Pearson. 3th Edition.

Jinlong, L., Hongyun, L., Jinpeng, X., 2013, Experimental study of corrosion behavior for burnished aluminum alloy by EWF, EBSD, EIS and Raman spectra, Appl. Surf. Sci., Vol. 273, p. 192–198.

Jinlong, L., Hongyun, L., Tongxiang, L., 2016, Investigation of microstructure and corrosion behavior of burnished aluminum alloy by TEM, EWF, XPS and EIS techniques, Mater. Res. Bull., Vol. 83, p. 148–154.

OpenCV, 2023, https://opencv.org/about/.

Pu, Z., Yang, S., Dillon, O.W., Puleo, D.A., Jawahir, I.S., 2011, Cryogenic burnishing of AZ31B Mg alloy for enhanced corrosion resistance, Magnes. Technol., 2011, p. 1–6.

Saldaña-Robles, Alberto., Plascencia-Mora, H., Aguilera-Gómez, E., Saldaña-Robles, Adriana., Marquez-Herrera, A., Diosdado-De la Peña, J. A., 2018, Influence of ball-burnishing on roughness, hardness and corrosion resistance of AISI 1045 steel, Surface and Coatings Technology, Vol. 339, p. 191-198.

Schulze, 2006, Modern mechanical surface treatment: states, stability, effects, Wiley-VCH, 2006.

Shreir, L.L., Jarman, R.A., Burstein, G.T., 1994, Corrosion, Butterworth Heinemann, 3th Edition, Vol. 1.

Summerfield, M., 2010, Programming in Python 3: A Complete Introduction to the Python Language, 2th Edition. Addison-Wesley.

6. RESPONSIBILITY NOTICE

The authors are the only responsible for the printed material included in this paper.